CFD simulations of MHD effects on mixed convectional flow in a lid-driven square cavity with square cylinder using Casson fluid

Article *in* Numerical Heat Transfer Fundamentals · June 2024

DOI: 10.1080/10407790.2024.2365890

CITATIONS
3

READS
120

2 authors:

Yasir Turabi
COMSATS University Islamabad
5 PUBLICATIONS **26** CITATIONS
SEE PROFILE

Shahzad Munir
COMSATS University Islamabad
32 PUBLICATIONS **367** CITATIONS
SEE PROFILE

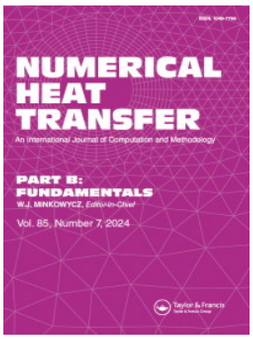

Taylor & Francis
Taylor & Francis Group

Numerical Heat Transfer, Part B: Fundamentals
An International Journal of Computation and Methodology

ISSN: (Print) (Online) Journal homepage: www.tandfonline.com/journals/unhb20

CFD simulations of MHD effects on mixed convectional flow in a lid-driven square cavity with square cylinder using Casson fluid

Yasir Ul Umair Bin Turabi & Shahzad Munir

To cite this article: Yasir Ul Umair Bin Turabi & Shahzad Munir (18 Jun 2024): CFD simulations of MHD effects on mixed convectional flow in a lid-driven square cavity with square cylinder using Casson fluid, Numerical Heat Transfer, Part B: Fundamentals, DOI: 10.1080/10407790.2024.2365890

To link to this article: https://doi.org/10.1080/10407790.2024.2365890

NUMERICAL HEAT TRANSFER, PART B: FUNDAMENTALS
https://doi.org/10.1080/10407790.2024.2365890

CFD simulations of MHD effects on mixed convectional flow in a lid-driven square cavity with square cylinder using Casson fluid

Yasir Ul Umair Bin Turabi and Shahzad Munir

Department of Mathematics, COMSATS University Islamabad, Pakistan

ABSTRACT

Enclosure design significantly impacts thermal engineering processes and devices, including electronic devices, thermal exchangers, power engines, heating systems, solar panels, and nuclear power plants. The square cavity with variable aspect ratios is utilized for multi-objective optimization and improved thermal performance of microchannels. Cold cylinders in square enclosures are often utilized to reduce energy loss in micro heat sinks and heat exchangers. So, article's main objective is to investigate concurrent characteristics of external and internal forces on a Casson fluid contained in a square cavity with magnetohydrodynamics (MHD). A square cylinder is embedded in the middle of the enclosure, and an inclined magnetic field with angle φ is applied. The upper lid is assumed to be inertially driven by a constant amount of slipping velocity, and a thermal state is disturbed by assuming uniform temperature at the left wall while the right wall and embedded cylinder are cool. The finite element method (FEM) based open-source software renowned as COMSOL Multiphysics is utilized to solve the non-dimensionalized momentum and energy equations. This study uses the square enclosure to study essential factors, such as the Casson parameter β, Hartmann number Ha, Reynolds number Re, and Grashof number Gr. The findings reveal that the kinetic energy at $\beta = 10$ is 12.22 times greater than that of $\beta = 0.1$ at $Ha = 0$. It is observed that Ha, β, and Gr have a direct impact on the local Nusselt number. Fluid kinetic energy increases as Gr increases while it decreases as Re increases. This study shows how obstacles of various shapes and temperature conditions have an essential impact on handling heat transfer characteristics.

ARTICLE HISTORY
Received 4 December 2023
Revised 31 May 2024
Accepted 4 June 2024

KEYWORDS
Casson fluid; embedded cylinder; FEM; MHD; mixed convection

1. Introduction

Due to its numerous applications in science, engineering, and industry, the study of heat transfer is critically important. The production of textiles, phase-changing materials, cooling electronic equipment, and heating and air conditioning systems in homes and automobiles all depend on the study of heat transfer. Over the years, these applications have prompted experimental and theoretical investigations into heat transfer mechanisms by researchers. This has saved time and money in the field and led to significant advancements. For instance, researchers have investigated heat transmission through various geometries of Newtonian and non-Newtonian fluids. Numerous studies have been published in this area because of the attention these investigations have received from the research community [1–9].

CONTACT Shahzad Munir shahzad_munir@comsats.edu.pk Department of Mathematics, COMSATS University Islamabad, park road, Tarlai Kalan, Islamabad 44000, Pakistan.

Nomenclature

FEM	finite element method	*Ha*	Hartmann number
B_0	*Magnetic field strength*	σ	Electrical conductivity
u, v	dimensional velocities components	k	thermal conductance
x, y	dimensional coordinates	β_T	Coefficient of heat expansion
$\bar{U}$, $\bar{V}$	nondimensional velocities components	T_h	hot temperature
$\bar{X}$, $\bar{Y}$	nondimensional coordinates	T_c	*cold temperature*
g	Gravitational acceleration	L	Cavity length
u_{lid}	moving wall	Re	Reynolds number
ρ	density	*Gr*	Grashof number
μ	dynamic viscosity	φ	magnetic field inclination
p	pressure	*Pr*	Prandtl number
C_p	specific heat	*Nu*	local Nusselt number
T	dimensional temperature	*K.E.*	total kinetic energy
P	nondimensional pressure	Nu_{avg}	average Nusselt number
θ	nondimensional temperature		
β	Casson parameter		

This phenomenon is typically called mixed convection when free and forced convection co-occur during the convection process. In this flow phenomenon, free and forced convection properties are of similar magnitude. Mixed convection occurs when the buoyant force significantly influences an enforced flow mechanism and inversely. Numerous specialists have developed mathematically, and tentatively blended convection streams and intensity move in different mathematical nooks, and research works are progressing for better investigation. The researchers evaluated a range of enclosure geometries due to their practical applicability in technological and engineering fields, for example, nuclear reactor factors, solar power storing, extracting oil, crystal development, electronic device cooling purposes, and thermal exchangers [10–12]. In addition, the high bottom wall temperature relative to its equivalent at the top produces the effect of free convection. They found that the frequency of dimensionless lid oscillations and the range of Re, Grashof numbers (Gr) affect heat transfer properties and fluid flow. Heat-conducting substances and cavity configurations block the concurrent flow of convective and thermal transfer in enclosures with various relative entrance and exit positions, and these factors can all impact convective flow. Shuja *et al.* [13] examined mixed convection in a square cavity caused by a rectangular body that generated heat. They noticed the consequence of outlet port location and perspective proportion on the intensity move qualities in the cavity. Their initial conclusion was that aspect ratios and the location of the outlet seaport are significantly exaggerated. Hsu and Sg [14] conducted a computational analysis on mixed convection thermal transport in a rectangle cavity with distinct heating sources on the bottom wall. According to Merrikh [15] investigation, the effects of blockage two can be mitigated by positioning a rigid body close to the walls. Contrasting and fenced-in areas having no obstructions, they additionally saw that the pace of intensity move might upgrade by setting fewer guide stuff. Hussein *et al.* [16] examined the streamlined and thermal features of laminar free and forced convective movement of tiny particles inside an inclination square using FDM.

Several geometric forms with different boundary conditions have also been studied in lid-driven cavities, where magnetohydrodynamics (MHD) significantly affect such shapes. Owing to its progressive applications in science and technology, including forced and mixed convection flow, processing food, food preparation, oil technologies, nuclear reactor technologies, air conditioning flow, heat transfer, food cooling, solar panel sheets, Solar power systems, mixed

conduction, forced conduction, as well as the transfer of heat in cavities, it has been thoroughly studied. Sheremet *et al.* [17] carried out a computer investigation to examine the impact of *Ha* and attractive configuration on strength increase processes. They discovered that when the *Ha* grows, the heat transport rate decreases, inhibiting convective flow. Convection motion intensifies as the position angle rises. The effects of a magnetic field, heat transfer, and entropy production on fluid flow were investigated by Dutta *et al.* [18]. They found this for increasingly substantial Rayleigh values ($Ra > 10^5$). The Hartmann number decreases substantially with the heat transmission rate. Bondareva *et al.* [19] demonstrate that the shape, game strategy, and Hartmann number of a bent porous nook may all have an impact on heat transfer. Further research on MHD in an enclosure may be found in references [11,20–24].

In mechanical and engineering applications, non-Newtonian liquids are more useful than Newtonian liquids. These liquids are employed in a variety of applications, including food production, metallurgical techniques, fuel extraction from crude oil, cycle entry, and biomedical activities [25]. Consequently, analysts are becoming more fascinated by the complex issue of non-Newtonian liquids. Certain substances exhibit non-Newtonian behavior when subjected to pressure, including but not limited to dirt, muck, catsup, blood, honey, colors, oozing, concentrated chocolate, egg whites, and mustard. Because of the complicated flow behavior of non-Newtonian liquids, no one model can fully represent all their properties. Numerous flow models have been proposed to better understand how these fluids move [26–29]. Viscoelastic fluids have attracted a great deal of attention among these models. These fluids represent a unique family of non-Newtonian materials that only flow when yield stress that is when pressures exceed a predefined threshold occurs. It's even more astounding than the yield stress value because they respond to stress like liquids. The behavior of viscoelastic fluid flow has been characterized by a few flow models [30–32]. Recently, the Casson fluid has drawn a lot of interest as one non-Newtonian fluid. A comprehensive examination of Casson fluid through various shapes under different conditions is accessible in these research articles [33–37].

Based on a literature study, it is determined that mixed convection heat transfer in liquid enclosures is essential for current research. Although there are several research on heated cylinders in enclosures, there is a lack of research on the heat and flow properties of fluids with cold cylinders. Therefore, this study aims to address this gap by assuming a Casson fluid under an inclined magnetic field contained in a square cavity with the addition of cold square obstacles. Additionally, cylinders in enclosures are widely used in civil and industrial engineering applications, including interior energy management, shaft cooling, bearings lubrication, and food manufacturing. Thermal management in enclosures may be improved by employing a cylinder with different thermal distributions [38–43]. The finite element method (FEM) based open-source software renowned as COMSOL multiphysics is utilized for numerical simulations. This article provides an in-depth look at the effects of the Casson parameter β, Hartmann number *Ha*, Reynolds number Re, and Grashof number *Gr* in a square cavity with square cylinders and an inclined magnetic field φ.

2. Mathematical modeling

2.1. Problem formulation

Consider a non-Newtonian Casson fluid flowing steady laminar, incompressible flow within a square cavity of width L, as depicted in Figure 1. The cavity origin point $(0, 0)$ is located at the bottom-left corner of the cavity. The characteristic length L is taken as 1 for the purpose of non-dimensionalization. Inertial forces are introduced into this situation by providing a lid-driven velocity of magnitude while keeping all other walls at rest. The square cylinder is embedded in the

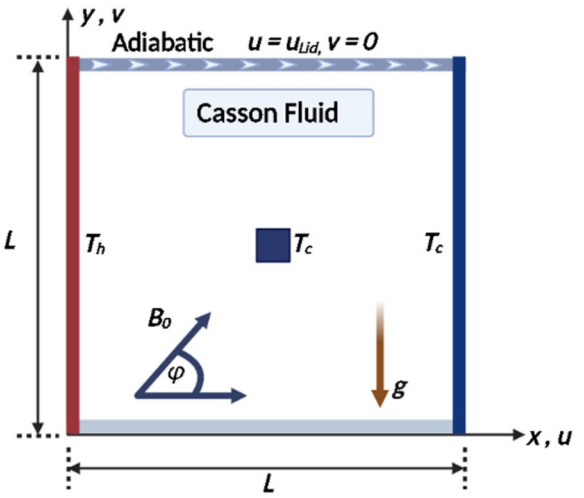

Figure 1. Geometry of the problem.

center $C(0.5, 0.5)$ of the cavity, and its surface is cold T_c. The horizontal side walls are adiabatic, with the left wall maintaining a hot temperature T_h and the right wall maintains a cold temperature T_c. An inclined magnetic field B_0 is placed at an angle of (φ) to the horizontal. Flow occurs in the enclosure because of the temperature gradient and motions of the top wall.

2.2. Governing equations

The governing equations of momentum and energy equation are as follows [44–46].

- Continuity equation

$$\frac{\partial u}{\partial x}+\frac{\partial v}{\partial y}=0 \tag{1}$$

- Transport of momentum

$$u\frac{\partial u}{\partial x}+v\frac{\partial u}{\partial y}=-\frac{1}{\rho}\frac{\partial p}{\partial x}+\frac{\mu}{\rho}\left(1+\frac{1}{\beta}\right)\left(\frac{\partial^2 u}{\partial x^2}+\frac{\partial^2 u}{\partial y^2}\right)+\frac{B_0\sigma}{\rho}\left(v\sin\varphi\cos\varphi-u\sin^2\varphi\right) \tag{2}$$

$$u\frac{\partial v}{\partial x}+v\frac{\partial v}{\partial y}=-\frac{1}{\rho}\frac{\partial p}{\partial y}+\frac{\mu}{\rho}\left(1+\frac{1}{\beta}\right)\left(\frac{\partial^2 v}{\partial x^2}+\frac{\partial^2 v}{\partial y^2}\right)+\frac{B_0\sigma}{\rho}\left(u\sin\varphi\cos\varphi-v\sin^2\varphi\right)+g\beta_T(T-T_0) \tag{3}$$

- Transport of energy

$$u\frac{\partial T}{\partial x}+v\frac{\partial T}{\partial y}=\frac{k}{(\rho C_p)}\left(\frac{\partial^2 T}{\partial x^2}+\frac{\partial^2 T}{\partial y^2}\right) \tag{4}$$

Boundary conditions of momentum:

$$\left.\begin{array}{ll} u(x,L)=1 & \text{(upper wall)} \\ u(x,0)=v(x,0)=u(0,y)=v(0,y) \;=\; u(L,y)=v(L,y)=v(x,L)=0 & \text{(remaining wall)} \end{array}\right\} \tag{5}$$

Boundary conditions of temperature:

$$\left.\begin{array}{ll} T(0,y)=1, & \text{(left wall)} \\ T(L,y)=0, & \text{(Right wall)} \\ \dfrac{\partial T}{\partial y}(x,0)=\dfrac{\partial T}{\partial y}(x,L)=0 & \text{(remaining wall)} \end{array}\right\} \tag{6}$$

Boundary conditions at the surface of the square cylinder:

$$u=v=T=0 \tag{7}$$

Dimensionless parameters and variables:

$$\begin{gathered} \bar{X}=\frac{x}{L},\ \bar{Y}=\frac{y}{L},\ \bar{U}=\frac{u}{u_{Lid}},\ \bar{V}=\frac{v}{u_{Lid}},\ \bar{P}=\frac{p}{\rho u_{Lid}^2},\ \theta=\frac{T-T_c}{T_h-T_c},\ \upsilon=\frac{\mu}{\rho},\alpha=\frac{k}{(\rho C_p)}, \\ \mathrm{Re}=\frac{u_{Lid}L}{\upsilon},\mathrm{Pr}=\frac{\upsilon}{\alpha},Gr=\frac{g\beta_T(T_h-T_c)L^3}{\upsilon^2},Ha=B_0L\sqrt{\frac{\sigma}{\mu}},Ri=\frac{Gr}{\mathrm{Re}^2} \end{gathered} \tag{8}$$

Using the above dimensionless parameters, Eqs. (1)–(4) become nondimensionalized governing equations:

$$\frac{\partial \bar{U}}{\partial \bar{X}}+\frac{\partial \bar{V}}{\partial \bar{Y}}=0 \tag{9}$$

$$\bar{U}\frac{\partial \bar{U}}{\partial \bar{X}}+\bar{V}\frac{\partial \bar{U}}{\partial \bar{Y}}=-\frac{\partial \bar{P}}{\partial \bar{X}}+\frac{1}{\mathrm{Re}}\left(1+\frac{1}{\beta}\right)\left(\frac{\partial^2 \bar{U}}{\partial \bar{X}^2}+\frac{\partial^2 \bar{U}}{\partial \bar{Y}^2}\right)+\frac{Ha^2}{\mathrm{Re}}\left(\bar{V}\sin\varphi\cos\varphi-\bar{U}\sin^2\varphi\right) \tag{10}$$

$$\begin{aligned} \bar{U}\frac{\partial \bar{V}}{\partial \bar{X}}+\bar{V}\frac{\partial \bar{V}}{\partial \bar{Y}}=&-\frac{\partial \bar{P}}{\partial \bar{Y}}+\frac{1}{\mathrm{Re}}\left(1+\frac{1}{\beta}\right)\left(\frac{\partial^2 \bar{V}}{\partial \bar{X}^2}+\frac{\partial^2 \bar{V}}{\partial \bar{Y}^2}\right)+\frac{Ha^2}{\mathrm{Re}}\left(\bar{U}\sin\varphi\cos\varphi-\bar{V}\sin^2\varphi\right) \\ &+\frac{Gr}{\mathrm{Re}^2}\theta \end{aligned} \tag{11}$$

$$\bar{U}\frac{\partial \theta}{\partial \bar{X}}+\bar{V}\frac{\partial \theta}{\partial \bar{Y}}=\frac{1}{\mathrm{PrRe}}\left(\frac{\partial^2 \theta}{\partial x^2}+\frac{\partial^2 \theta}{\partial y^2}\right) \tag{12}$$

Nondimensional boundary conditions of momentum:

$$\left.\begin{array}{ll} \bar{U}(\bar{X},1)=1, & \text{(upper wall)} \\ \bar{U}(\bar{X},0)=\bar{V}(\bar{X},0)=\bar{U}(0,\bar{Y})=\bar{V}(0,\bar{Y})\ =\bar{U}(1,\bar{Y})=\bar{V}\ (1,\bar{Y})=\bar{V}(\bar{X},1)=0 & \text{(remaining wall)} \end{array}\right\} \tag{13}$$

Nondimensional boundary conditions of temperature:

$$\left.\begin{array}{ll} \theta(0,\bar{Y})=1, & \text{(left wall)} \\ \theta(1,\bar{Y})=0, & \text{(Right wall)} \\ \dfrac{\partial \theta}{\partial \bar{Y}}\ (\bar{X},0)=\dfrac{\partial \theta}{\partial \bar{Y}}\ (\bar{X},1)=0 & \text{(remaining wall)} \end{array}\right\} \tag{14}$$

Nondimensional boundary conditions on the square cylinder's surface:

$$\bar{U}=\bar{V}=\theta=0$$

The local Nusselt number, average Nusselt number, and Total kinetic energy are obtained by:

$$Nu=\left(-\frac{\partial \theta}{\partial \bar{X}}\right)_{\bar{X}=0} \tag{15}$$

$$Nu_{avg}=\int_0^1 Nu\ dY \tag{16}$$

$$K.E = \frac{1}{2}\int_{\Omega} \|U\|^2 d\Omega \tag{17}$$

Where $U = (\bar{U}, \bar{V})$ is the velocity vector.

3. Numerical method and grid independence

In this work, nondimensional Eqs. (9)–(12) with boundary conditions (13) and (14) are solved numerically using a FEM-based open-source software renowned as COMSOL. The FEM is a mathematical tool for computing an approximative solution for some basic differential equations that cannot be resolved analytically. This methodology begins by separating the problem domain into irregular triangular finite element meshes. This method starts with finite elements meshing the issue region into irregular triangle shapes. Since the basic differential equations for various fluid flow problems are composed of several connected nonlinear equations, this strategy uses consecutive linearization methods to solve the equations. Iterative approaches are often used to solve the linear structures from this approach. The nonlinear administering fractional differential conditions, especially the mass, force, and energy conditions, are then securely transformed into an arrangement of essential conditions using the Galerkin Leftover process. The integration essential for each iteration of these equations is performed using the Gaussian iteration method. The solution does not specify how many hubs and lattice types should be kept for each logarithmic. The resultant nonlinear equations are adjusted by imposing boundary conditions. The Newton–Raphson transform is used to convert these updated nonlinear equations into linear algebraic equations. To extract the variables while meeting the convergent criteria, these linear equations are solved using the triangle factoring approach. The nonlinear iterations are based on the following convergence condition.

$$\left|\frac{\chi^{n+1} + \chi^{n}}{\chi^{n+1}}\right| < 10^{-6}$$

where χ characterizes the general solution component. Figure 2 shows the computational mesh at a finer grid level. Figure 3 describes the stages involved in the FEM.

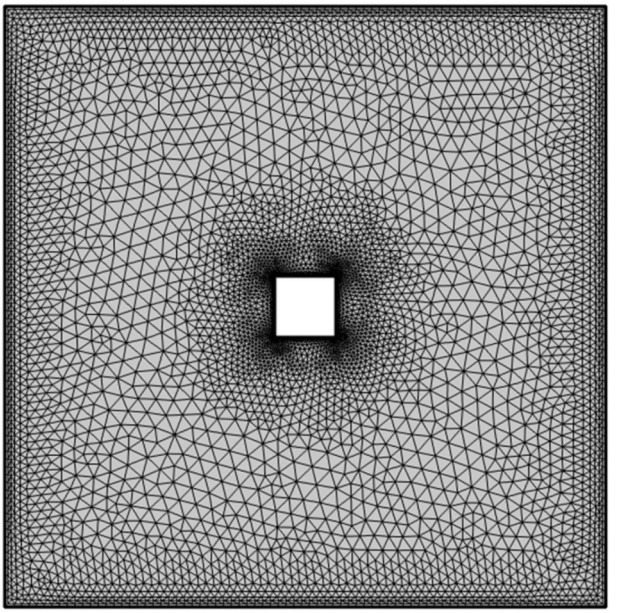

Figure 2. Finer grid for cavity with a square block placed at C (0.5, 0.5).

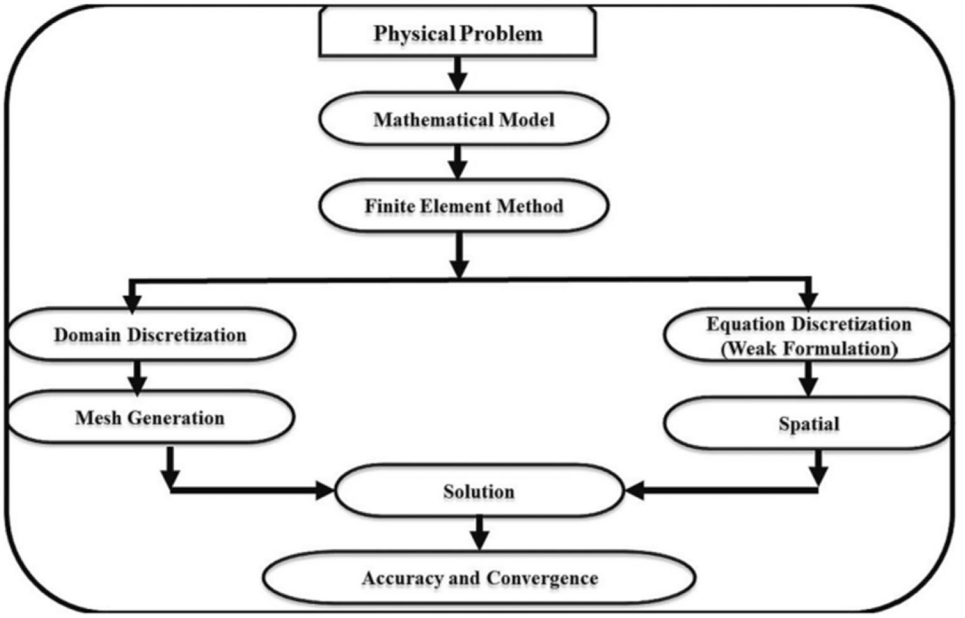

Figure 3. Diagram showing the finite element method's workflow.

Table 1. Grid convergence analysis for the Nu_{avg} and $K.E_{avg}$.

Gird	NEL	DOFs	Nu_{avg}	$K.E_{.avg}$
1	372	976	1.7474	0.045174
2	612	1,576	1.7349	0.045034
3	966	2,380	1.7276	0.045257
4	1,688	4,064	1.7212	0.045289
5	2,496	5,872	1.7183	0.045336
6	3,934	8,964	1.7163	0.045449
7	9,960	22,216	1.7137	0.045505
8	24,746	53,948	1.7129	0.045535

3.1. Grid test

Several grids are utilized to demonstrate the efficiency of the acquired findings for the cases of $\beta = 0.1$, $Ha = 25$, $\mathrm{Pr} = 6.8$, $Gr = 10^3$, $\mathrm{Re} = 1$, and $\varphi = 0$. As seen in Table 1. Consequently, the total number of elements (NEL) and degrees of freedom (DOF) vary from 372 to 24,746 and 976 to 53,948, respectively. As can be seen, the difference between the mean Nusselt number figures is small for the last two grids. Consequently, DOFs of 22,216 and NEL of 9,960 may assure gird independence and the numerical findings are based on these DOFs and NEL.

3.2. Comparison

A qualitative comparison between the present results and the results of Mehmood *et al.* [20] is provided in Figure 4. From these comparisons and percentage deviation, we concluded that the available and present findings are in excellent agreement, validating the developed scheme for the considered problem.

4. Results and discussions

This section lists the selective findings obtained using the streamlines, isothermal. Figure 5 shows how the various Casson parameters β affect the streamlines and isotherms patterns. Two vortices

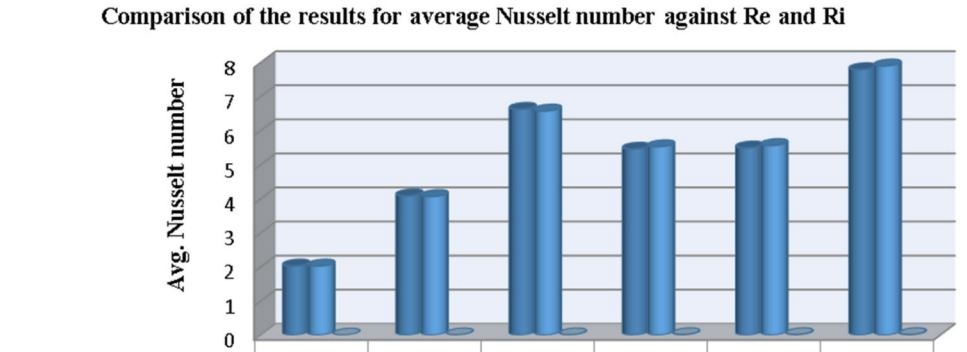

	Re=100	Re=400	Re=1000	Ri=0.1	Ri=1	Ri=10
Present results	2.03	4.09	6.63	5.4611	5.4957	7.7951
Mehmood et al. [20]	2.03	4.07	6.58	5.5317	5.5684	7.9029
Percentage deviation (%)	0%	0.49%	0.76%	1.27%	1.30%	1.37%

Figure 4. Comparison of the present results with Mehmood *et al*. [20] for Nu_{avg} against Re and Ri.

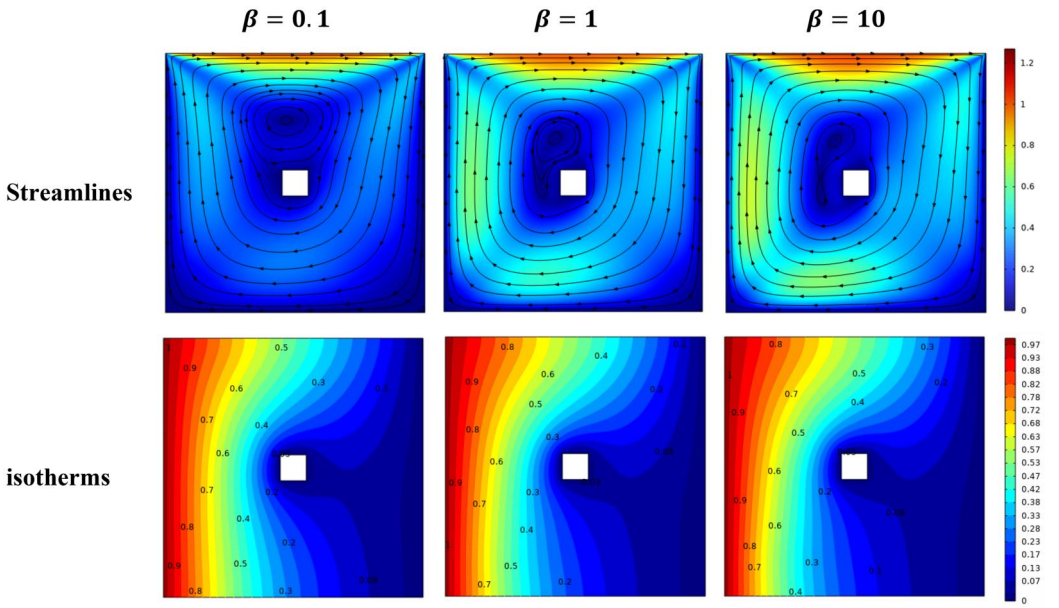

Figure 5. Streamlines and isotherms form different β for $Ha = 25$, $\Pr = 6.8$, $Gr = 10^3$, $\mathrm{Re} = 1$, and $\varphi = 0$.

can be noticed created around the cylinder, and the fluid rotates in a clockwise direction because of the motions of the top wall and elevated temperature of the left wall and the reduced temperature of the right wall. Furthermore, as the increased Casson fluid parameter β identifies the additional fluid viscosity and causes a drop in the effective viscosity of the working fluid, streamlines become more intense, and the velocity of the flow movement is significantly raised for rising. As a result, at lower $\beta = 0.1$, the streamline distribution has a lesser magnitude, which strengthens with increasing strength at higher $\beta = 10$. However, the isothermal contours show no substantial change when the Casson parameter values are increased. Figure 6 displays the Nusselt number in different values of Casson parameters β. As can be seen, the Casson parameters of 10 produced the most significant Nusselt number. Furthermore, the findings revealed that the Casson parameters immediately impact the Nusselt number. Table 2 displays the average Nu and $K.E.$ values for

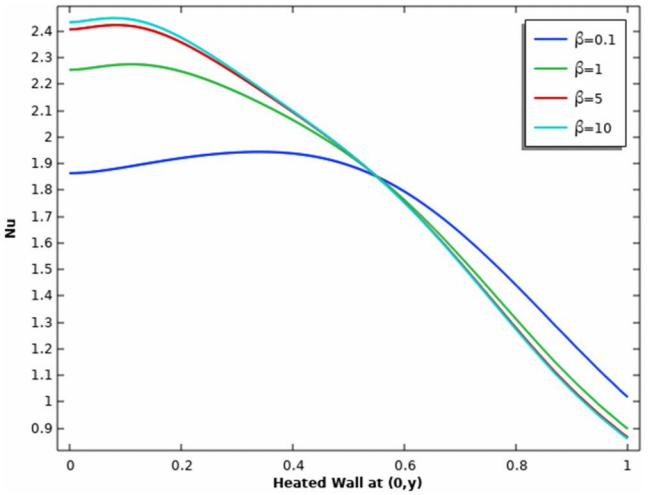

Figure 6. The *Nu* variations on the heated wall for various parameters of β for $Ha = 25$, $\mathrm{Pr} = 6.8$, $Gr = 10^3$, $\mathrm{Re} = 1$, and $\varphi = 0$.

Table 2. Mean Nusselt number and *K.E.* variations for different parameters of β and *Ha* values for $\mathrm{Pr} = 6.8$, $Gr = 10^3$, $\mathrm{Re} = 1$, and $\varphi = 0$.

	Nu_{avg}				$K.E._{avg}$			
Ha	$\beta = 0.1$	$\beta = 1$	$\beta = 5$	$\beta = 10$	$\beta = 0.1$	$\beta = 1$	$\beta = 5$	$\beta = 10$
0	1.7704	2.3505	2.6983	2.7646	0.075188	0.47889	0.83916	0.91939
25	1.7137	1.7994	1.8309	1.8362	0.045505	0.081621	0.095586	0.098016
50	1.6705	1.6679	1.6678	1.6678	0.025787	0.022958	0.022456	0.022392
75	1.6561	1.6488	1.6475	1.6473	0.019517	0.014395	0.013209	0.013024
100	1.65	1.6434	1.6424	1.6422	0.016547	0.011456	0.010288	0.010103

various *Ha* and β. As can be seen, the most significant average *Nu* number has been found in $\beta = 10$ and $Ha = 0$, which is 2.7646. On the other hand, findings revealed that *K.E.* in the cases of $\beta = 10$ and $Ha = 0$ rise 12.22 times higher than in the case of $\beta = 0.1$ and $Ha = 0$.

Figure 7 shows how the various Hartmann number *Ha* affect the streamlines and isotherms patterns. The increasing number of vortices with higher Hartmann numbers *Ha* is due to the magnetic field's stronger impact on the flow. As *Ha* rises, the fluid resists lateral motion and streamlines its flow toward the top wall due to the increasing dominance of magnetic forces. Although *Ha* has a considerable effect on the flow patterns, the isotherm contours' little alterations indicate that its effect on the enclosure's temperature distribution is less than that of the magnetic field on flow behavior. Figure 8 displays the Nusselt number in different values of Hartmann number *Ha*. By increasing the Hartmann number, the Nusselt number behave increasing and decreasing effects. The reduction in the Nusselt number in the upper area of the cavity as the *Ha* increases is due to the stronger Lorentz forces increased suppression of fluid motion, which restricts convective heat transfer. Conversely, the lower area of the cavity Nusselt number increases due to the lesser influence of Lorentz forces allowing for increased fluid motion and improved convective heat transfer along the cavity bottom wall. As can be seen, the Hartmann number *Ha* of 0 produced the greatest Nusselt number. Table 3 displays the average *Nu* and *K.E.* values for various *Ha* and *Re*. As can be seen, the greatest average *Nu* number has been found in $Re = 100$ and $Ha = 0$, which is 7.0417. Furthermore, it is clear that $Re = 1$ and $Ha = 0$ produced the most K.E., while $Re = 50$ and $Ha = 100$ produced the lowest

Figure 9 shows how the various Reynolds number Re affect the streamlines and isotherms patterns. The obtained streamlines demonstrate that by raising Re, the force of convection grows

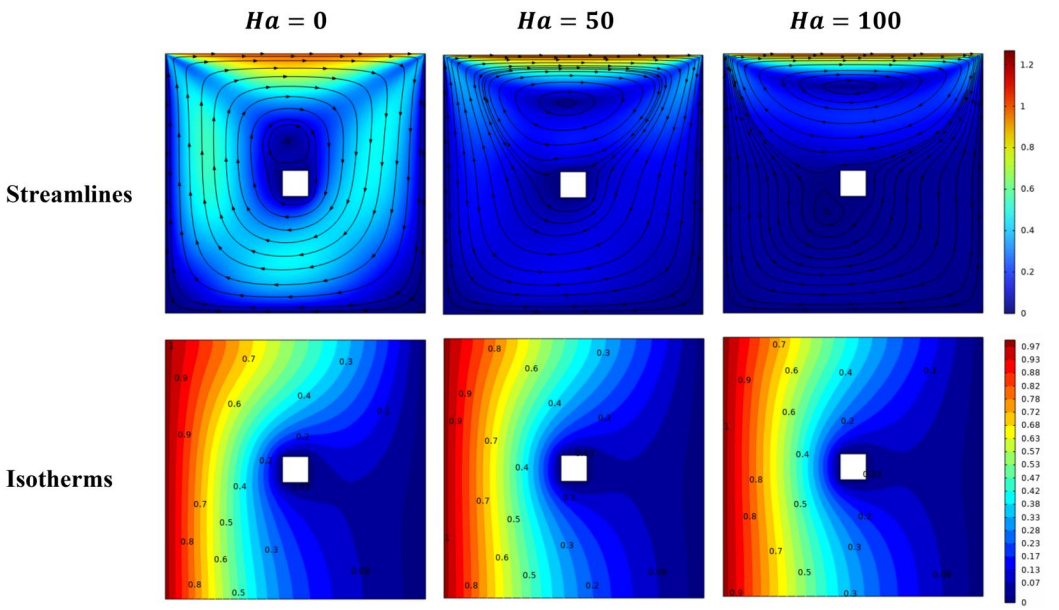

Figure 7. Streamlines and isotherms form different *Ha* for $\beta = 0.1$, Pr $= 6.8$, $Gr = 10^3$, Re $= 1$, and $\varphi = 0$.

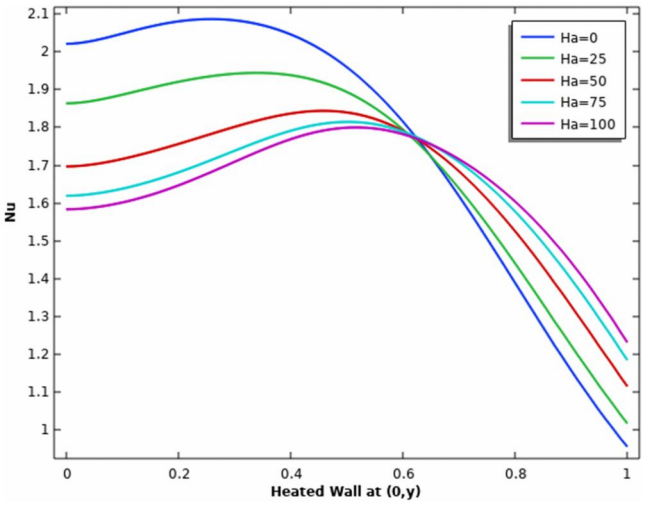

Figure 8. The *Nu* variations on the heated wall for various parameters of *Ha* for $\beta = 0.1$, Pr $= 6.8$, $Gr = 10^3$, Re $= 1$, and $\varphi = 0$.

and takes over natural convection. Because force convection is formed due to upper lid movement, slip velocity significantly impacts the motion observed from vortex generation. The intensity of clockwise rotation rises with increasing Re, as predicted, owing to dominance over natural convection. The same effect can be seen in isotherm patterns. As the Re enhance, the cavity's isotherm becomes horizontal. Figure 10 illustrates the fluctuation of the Nusselt number for various Reynolds number Re values. The finding showed that the most significant and lowest Nusselt number occurred in Re of 100 and 1. The rise in Nusselt number with increasing Reynolds number *Re* is due to increased fluid velocity inside the enclosure. As Re rises, the flow transforms from laminar to turbulent, increasing heat transmission through enhanced mixing and convective

Table 3. Mean nusselt number and *K.E.* variations for different parameters of Ha and er values for Pr = 6.8, $Gr = 10^3$, and $\varphi = 0$.

	Nu_{avg}				$K.E._{avg}$			
Ha	Re = 1	Re = 10	Re = 50	Re = 100	Re = 1	Re = 10	Re = 50	Re = 100
0	1.7704	3.0879	5.5587	7.0417	0.075188	0.03129	0.03028	0.030262
25	1.7137	2.8165	5.3614	6.8131	0.045505	0.025423	0.024873	0.024858
50	1.6705	2.5031	4.751	6.2459	0.025787	0.020614	0.020488	0.020485
75	1.6561	2.3413	4.2952	5.5076	0.019517	0.017869	0.017839	0.017842
100	1.65	2.2274	4.0996	5.2149	0.016547	0.015843	0.015831	0.015834

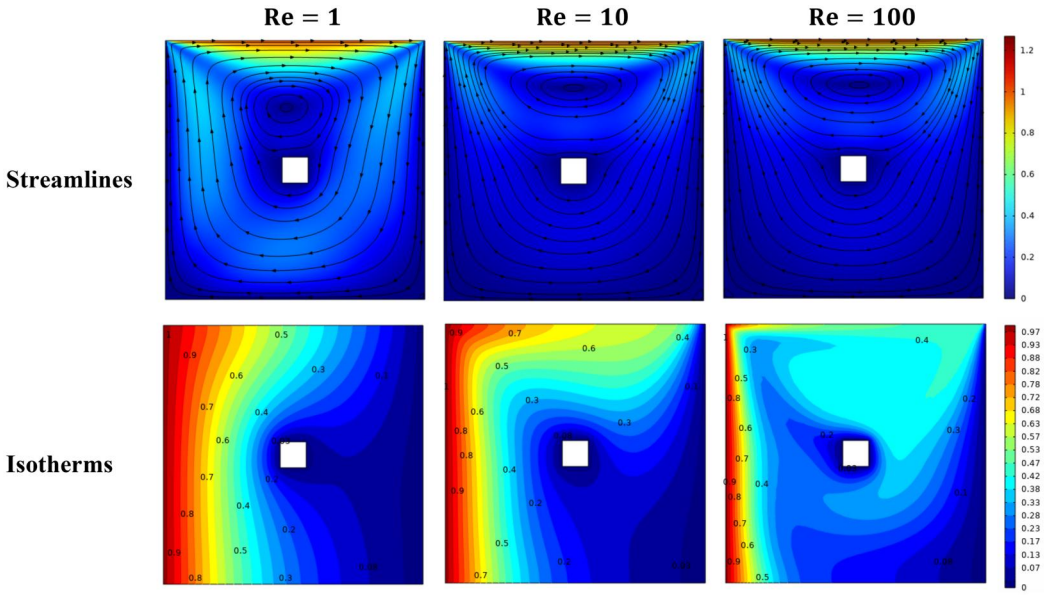

Figure 9. Streamlines and isotherms form different er for $Ha = 25$, Pr = 6.8, $Gr = 10^3$, $\beta = 0.1$, and $\varphi = 0$.

heat transfer. Table 4 shows how the average *Nu* and *K.E.* values for various φ and *Re* According to the results, the highest average *Nu* number was recorded in $\varphi = 45$ and Re = 100 and is equivalent to 6.8908, while the most significant average *K.E.* number was achieved in $\varphi = 75$ and Re = 1, and is equivalent to 0.04814.

Figure 11 shows how the various Grashof number *Gr* affects streamlines and isotherms patterns. It has been noticed that increasing *Gr* increases the effect of buoyant forces and generates a higher temperature differential between cold and hot walls. Raising *Gr* increases the temperature gradient since it indicates the buoyant to inertial forces ratio. It has also been shown that increasing *Gr* increases flow circulation. Subsequently, it is determined that as *Gr* gradually rises, buoyancy effects become more significant, resulting in symmetrical clockwise circulation at $Gr = 10^6$. Furthermore, two vortexes formed toward the lower corner of the left wall and the upper corner of the right wall. Figure 12 illustrates the fluctuation of the Nusselt number for various Grashof number *Gr* values. It has been noted that when the *Gr* increases, the Nusselt number also increases. The rise in *Gr* causes increased buoyant forces inside the enclosure, enabling enhanced fluid circulation and transfer of heat. The finding showed that the most significant and lowest Nusselt number occurred in *Gr* of 10^3. Table 5 shows how the average *Nu* and *K.E.* values for various φ and *Gr*. As can be seen, the most significant average *Nu* value has been found in $\varphi = 90$ and $Gr = 10^6$, and is equivalent to 9.9004, while the most significant average *K.E.* the number was achieved in $\varphi = 75$ and $Gr = 10^6$, and is equal to 48.528.

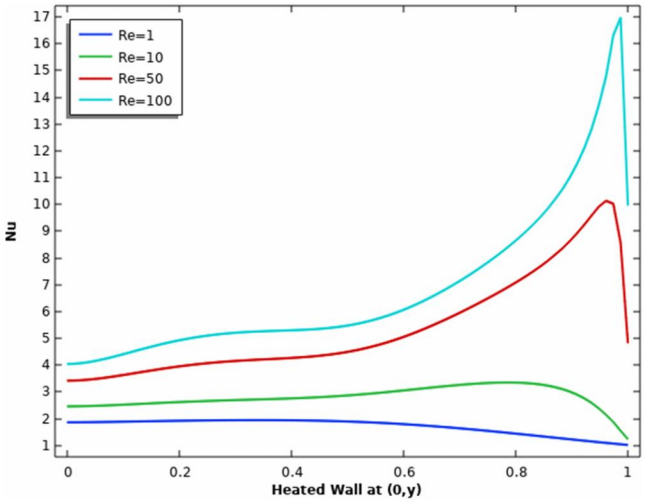

Figure 10. The *Nu* variations on the heated wall for various parameters of er for $Ha = 25$, $\Pr = 6.8$, $Gr = 10^3$, $\beta = 0.1$, and $\varphi = 0$.

Table 4. Mean nusselt number and *K.E.* variations for different parameters of Re and φ values for $\Pr = 6.8$, $Gr = 10^3$, $\beta = 0.1$, and $Ha = 25$.

	Nu_{avg}				$K.E._{avg}$			
φ	Re = 1	Re = 10	Re = 50	Re = 100	Re = 1	Re = 10	Re = 50	Re = 100
0	1.7137	2.8165	5.3614	6.8131	0.04550	0.02542	0.02487	0.02485
15	1.7147	2.8265	5.3883	6.8451	0.04597	0.02534	0.02477	0.02476
30	1.7166	2.8451	5.4171	6.8743	0.04676	0.02513	0.02452	0.02452
45	1.7188	2.8665	5.435	6.8908	0.04757	0.02491	0.02425	0.02426
60	1.7205	2.8836	5.4373	6.8905	0.04807	0.02473	0.02404	0.02405
75	1.7212	2.8921	5.4271	6.8749	0.04814	0.02460	0.02390	0.02390
90	1.7211	2.8912	5.41	6.8497	0.04793	0.02453	0.02385	0.02384

5. Conclusions

This research examines the heat transport characteristics of non-Newtonian Casson fluids flow in a 2-D square enclosure using COMSOL Multiphysics software. A cold square cylinder is inserted in the center of the cavity to manage heat and provide uniform heating at the left wall. The finding may have significant consequences for thermal engineering processes and equipment, including microelectronics, heat exchangers, power engines, micro heat sinks, and nuclear reactors. Numerous kinds of factors are used to observe changes in momentum and temperature distributions along streamlines and isotherm patterns. The following are some significant results of our present work:

- The kinetic energy at $\beta = 10$ is 12.22 times greater than that of $\beta = 0.1$ at $Ha = 0$.
- Hartmann number *Ha* and Casson parameters β have a direct impact on the local Nusselt number.
- An increase in the Grashof number increases thermal buoyancy forces, which enhances the Nusselt number.
- Deformation in isotherms and fluid flow circulations are generated against the increase in *Gr*.
- Fluid kinetic energy increases as Grashof number increases and decreases as Reynold number increases.

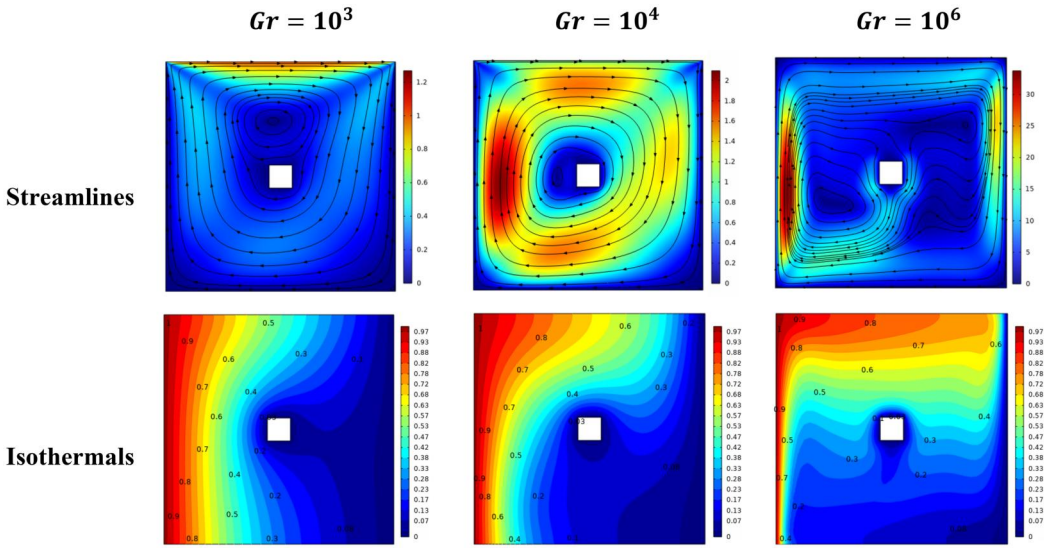

Figure 11. Streamlines and isothermals form different Gr for $Ha = 25$, $\mathrm{Pr} = 6.8$, $\mathrm{re} = 1$, $\beta = 0.1$, and $\varphi = 0$.

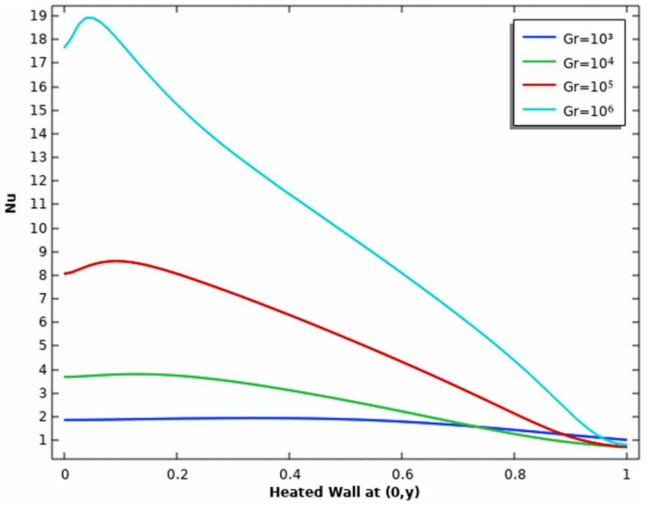

Figure 12. The Nu variations on the heated wall for various parameters of Gr for $Ha = 25$, $\mathrm{Pr} = 6.8$, $\mathrm{re} = 1$, $\beta = 0.1$, and $\varphi = 0$.

Table 5. Mean nusselt number and $K.E.$ variations for different parameters of Gr and φ values for $\mathrm{Pr} = 6.8$, $\mathrm{re} = 1$, $\beta = 0$, and $Ha = 25$.

	Nu_{avg}				$K.E._{avg}$			
φ	$Gr = 10^3$	$Gr = 10^4$	$Gr = 10^5$	$Gr = 10^6$	$Gr = 10^3$	$Gr = 10^4$	$Gr = 10^5$	$Gr = 10^6$
0	1.7137	2.5223	5.0899	9.8197	0.04550	0.60182	6.3401	46.687
15	1.7147	2.5344	5.1052	9.83	0.04597	0.61838	6.4641	47.054
30	1.7166	2.5479	5.1286	9.8482	0.04676	0.6345	6.5941	47.553
45	1.7188	2.5579	5.1541	9.8697	0.04757	0.64294	6.6921	48.057
60	1.7205	2.5609	5.1746	9.8888	0.04807	0.6399	6.7299	48.418
75	1.7212	2.557	5.1843	9.9001	0.04814	0.62784	6.6982	48.528
90	1.7211	2.5485	5.1806	9.9004	0.04793	0.61278	6.6079	48.353

Disclosure statement

No AI-assisted technology is used in the preparation of this manuscript.

Funding

There are no financial or personal interests to disclose.

ORCID

Shahzad Munir http://orcid.org/0000-0003-0666-4046

References

[1] G. K. Batchelor, "Heat transfer by free convection across a closed cavity between vertical boundaries at different temperatures," *Quart. Appl. Math.*, vol. 12, no. 3, pp. 209–233, 1954. DOI: 10.1090/qam/64563.

[2] J. P. Hartnett and M. Kostic, "Heat transfer to Newtonian and non-Newtonian fluids in rectangular ducts," *Adv. Heat Transf.*, vol. 19, pp. 247–356, 1989. DOI: 10.1016/S0065-2717(08)70214-4.

[3] B. Zalba, J. M. Marın, L. F. Cabeza and H. Mehling, "Review on thermal energy storage with phase change: materials, heat transfer analysis and applications," *Appl. Therm. Eng.*, vol. 23, no. 3, pp. 251–283, 2003. DOI: 10.1016/S1359-4311(02)00192-8.

[4] Y. Kai, *et al.*, "A case study of different magnetic strength fields and thermal energy effects in vortex generation of Ag-TiO2 hybrid nanofluid flow," *Case Stud. Therm. Eng.*, vol. 47, pp. 103115, 2023. DOI: 10.1016/j.csite.2023.103115.

[5] S. Ahmad, J. Cai and K. Ali, "Prediction of new vortices in single-phase nanofluid due to dipole interaction," *J. Therm. Anal. Calorim.*, vol. 147, no. 1, pp. 461–475, 2022. DOI: 10.1007/s10973-020-10237-5.

[6] R. Ayub, S. Ahmad, S. Ahmad, Y. Akhtar, M. M. Alam and O. Mahmoud, "Numerical assessment of dipole interaction with the single-phase nanofluid flow in an enclosure: a pseudo-transient approach," *Materials*, vol. 15, no. 8, pp. 2761, 2022. DOI: 10.3390/ma15082761.

[7] K. Ali, S. Ahmad, S. Ahmad, W. Jamshed, S. M. Hussain and E. S. M. Tag El Din, "Molecular interaction and magnetic dipole effects on fully developed nanofluid flowing via a vertical duct applying finite volume methodology," *Symmetry*, vol. 14, no. 10, pp. 2007, 2022. DOI: 10.3390/sym14102007.

[8] D. Chatterjee, B. Mondal and P. Halder, "Hydromagnetic mixed convective transport in a vertical lid-driven cavity including a heat conducting rotating circular cylinder," *Numer. Heat Transf. A*, vol. 65, no. 1, pp. 48–65, 2014. DOI: 10.1080/10407782.2013.812399.

[9] D. Chatterjee and S. Kumar Gupta, "Magnetohydrodynamic natural convection in a square enclosure with four circular cylinders positioned at different rectangular locations," *Heat Transf. Eng.*, vol. 38, no. 17, pp. 1449–1465, 2017. DOI: 10.1080/01457632.2016.1255078.

[10] O. Aydm, "Aiding and opposing mechanisms of mixed convection in a shear-and buoyancy-driven cavity," *Int. Commun. Heat Mass Transf.*, vol. 26, no. 7, pp. 1019–1028, 1999. DOI: 10.1016/S0735-1933(99)00091-3.

[11] S. Ray and D. Chatterjee, "MHD mixed convection in a lid-driven cavity including heat conducting solid object and corner heaters with Joule heating," *Numer. Heat Transf. A*, vol. 66, no. 5, pp. 530–550, 2014. DOI: 10.1080/10407782.2014.892399.

[12] D. Chatterjee and R. Mishra, "Numerical investigation of transient magnetohydrodynamic mixed convection in a ventilated cavity containing two heated circular cylinders," *Heat Transf. Eng.*, vol. 39, no. 12, pp. 1052–1066, 2018. DOI: 10.1080/01457632.2017.1358487.

[13] S. Z. Shuja, B. S. Yilbas and M. O. Iqbal, "Mixed convection in a square cavity due to heat generating rectangular body: effect of cavity exit port locations," *Int. J. Numer. Methods Heat Fluid Flow*, vol. 10, no. 8, pp. 824–841, 2000. DOI: 10.1108/09615530010359120.

[14] T. H. Hsu and W. A. Sg, "Mixed convection in a rectangular enclosure with discrete heat sources," *Numer. Heat Transf. A*, vol. 38, no. 6, pp. 627–652, 2000. DOI: 10.1080/104077800750021170.

[15] A. A. Merrikh, "Blockage effects in natural convection in differentially heated enclosures," *J. Enh. Heat Transf.*, vol. 8, no. 1, pp. 55–72, 2001. DOI: 10.1615/JEnhHeatTransf.v8.i1.50.

[16] A. K. Hussein, S. E. Ahmed, H. A. Mohammed and W. A. Khan, "Mixed convection of water-based nanofluids in a rectangular inclined lid-driven cavity partially heated from its left side wall," *J. Comput. Theor. Nanosci.*, vol. 10, no. 9, pp. 2222–2233, 2013. DOI: 10.1166/jctn.2013.3191.

[17] M. A. Sheremet, H. F. Oztop and I. Pop, "MHD natural convection in an inclined wavy cavity with corner heater filled with a nanofluid," *J. Magn. Magn. Mater.*, vol. 416, pp. 37–47, 2016. DOI: 10.1016/j.jmmm.2016.04.061.

[18] S. Dutta, N. Goswami, A. K. Biswas and S. Pati, "Numerical investigation of magnetohydrodynamic natural convection heat transfer and entropy generation in a rhombic enclosure filled with Cu-water nanofluid," *Int. J. Heat Mass Transf.*, vol. 136, pp. 777–798, 2019. DOI: 10.1016/j.ijheatmasstransfer.2019.03.024.

[19] N. S. Bondareva, M. A. Sheremet, H. F. Oztop and N. Abu-Hamdeh, "Heatline visualization of MHD natural convection in an inclined wavy open porous cavity filled with a nanofluid with a local heater," *Int. J. Heat Mass Transf.*, vol. 99, pp. 872–881, 2016. DOI: 10.1016/j.ijheatmasstransfer.2016.04.055.

[20] K. Mehmood, S. Hussain and M. Sagheer, "Mixed convection in alumina-water nanofluid filled lid-driven square cavity with an isothermally heated square blockage inside with magnetic field effect: introduction," *Int. J. Heat Mass Transf.*, vol. 109, pp. 397–409, 2017. DOI: 10.1016/j.ijheatmasstransfer.2017.01.117.

[21] S. Ahmad, H. Takana, K. Ali, Y. Akhtar, A. M. Hassan and A. E. Ragab, "Role of localized magnetic field in vortex generation in tri-hybrid nanofluid flow: a numerical approach," *Nanotechnol. Rev.*, vol. 12, no. 1, pp. 20220561, 2023. DOI: 10.1515/ntrev-2022-0561.

[22] D. Chatterjee, "MHD mixed convection in a lid-driven cavity including a heated source," *Numer. Heat Transf. A*, vol. 64, no. 3, pp. 235–254, 2013. DOI: 10.1080/10407782.2013.779191.

[23] D. Chatterjee, P. Halder, S. Mondal and S. Bhattacharjee, "Magnetoconvective transport in a vertical lid-driven cavity including a heat conducting square cylinder with Joule heating," *Numer. Heat Transf. A*, vol. 64, no. 12, pp. 1050–1071, 2013. DOI: 10.1080/10407782.2013.811955.

[24] S. Ahmad *et al.*, "Vortex generation due to multiple localized magnetic fields in the hybrid nanofluid flow–A numerical investigation," *Heliyon*, vol. 9, no. 7, pp. e17756, 2023. DOI: 10.1016/j.heliyon.2023.e17756.

[25] A. R. Ghigo, P. Y. Lagree and J. M. Fullana, "A time-dependent non-Newtonian extension of a 1D blood flow model," *J. Non-Newtonian Fluid Mech.*, vol. 253, pp. 36–49, 2018. DOI: 10.1016/j.jnnfm.2018.01.004.

[26] A. Chandra and R. P. Chhabra, "Influence of power-law index on transitional Reynolds numbers for flow over a semi-circular cylinder," *Appl. Math. Modell.*, vol. 35, no. 12, pp. 5766–5785, 2011. DOI: 10.1016/j.apm.2011.05.004.

[27] A. Chandra and R. P. Chhabra, "Laminar free convection from a horizontal semi-circular cylinder to power-law fluids," *Int. J. Heat Mass Transf.*, vol. 55, no. 11–12, pp. 2934–2944, 2012. DOI: 10.1016/j.ijheatmasstransfer.2012.02.034.

[28] N. Santhosh, G. Radhakrishnamacharya and A. J. Chamkha, "Flow of a Jeffrey fluid through a porous medium in narrow tubes," *J. Por. Media*, vol. 18, no. 1, pp. 71–78, 2015. DOI: 10.1615/JPorMedia.v18.i1.60.

[29] S. Aman, Q. Al-Mdallal and I. Khan, "Heat transfer and second order slip effect on MHD flow of fractional Maxwell fluid in a porous medium," *J. King Saud Univ. Sci.*, vol. 32, no. 1, pp. 450–458, 2020. DOI: 10.1016/j.jksus.2018.07.007.

[30] E. C. Bingham, *An Investigation of the Laws of Plastic Flow*. Washington, DC: US Government Printing Office, 1917.

[31] W. H. Herschel and R. Bulkley, "Measurement of consistency as applied to rubber-benzene solutions," *Am. Soc. Test Proc.*, vol. 26, no. 2, pp. 621–633, Jun. 1926. DOI: 10.1021/ie50177a019.

[32] N. Casson, *A Flow Equation for Pigment-Oil Suspensions of the Printing Ink Type*. In: Mill, C.C., Ed., Rheology of Disperse Systems, Pergamon Press, Oxford, pp. 84-104, 1959.

[33] Y. U. U. B. Turabi, S. Munir and A. Amin, "Numerical analysis of convective transport mechanisms in two-layer ternary (TiO2-SiO2-Al2O3) Casson hybrid nanofluid flow in a vertical channel with heat generation effects," *Numer. Heat Transf. A*, vol. 1, pp. 1–15, 2023. DOI: 10.1080/10407782.2023.2281542.

[34] Y. U. B. Turabi, A. Amin, S. Munir and U. Farooq, "Investigating flow features and heat/mass transfer in two-layer vertical channel with Gr-TiO2 hybrid nanofluid under MHD and radiation effects," *J. Magn. Magn. Mater.*, vol. 578, pp. 170800, 2023. DOI: 10.1016/j.jmmm.2023.170800.

[35] I. Ullah, T. A. Alkanhal, S. Shafie, K. S. Nisar, I. Khan, and O. D. Makinde, "MHD slip flow of Casson fluid along a nonlinear permeable stretching cylinder saturated in a porous medium with chemical reaction, viscous dissipation, and heat generation/absorption," *Symmetry*, vol. 11, no. 4, p. 531, 2019. DOI: 10.3390/sym11040531.

[36] B. Mahanthesh, B. J. Gireesha, N. S. Shashikumar, T. Hayat and A. Alsaedi, "Marangoni convection in Casson liquid flow due to an infinite disk with exponential space dependent heat source and cross-diffusion effects," *Results Phys.*, vol. 9, pp. 78–85, 2018. DOI: 10.1016/j.rinp.2018.02.020.

[37] A. S. Rao, S. Sainath, P. Rajendra and G. Ramu, "Mathematical modelling of hydromagnetic Casson non-Newtonian nanofluid convection slip flow from an isothermal sphere," *Nonlinear Eng.*, vol. 8, no. 1, pp. 645–660, 2019. DOI: 10.1515/nleng-2018-0016.

[38] E. Kossecka and J. Kosny, "Influence of insulation configuration on heating and cooling loads in a continuously used building," *Energy Build.*, vol. 34, no. 4, pp. 321–331, 2002. DOI: 10.1016/S0378-7788(01)00121-9.

[39] M. Ozel, "Thermal performance and optimum insulation thickness of building walls with different structure materials," *Appl. Therm. Eng.*, vol. 31, no. 17–18, pp. 3854–3863, 2011. DOI: 10.1016/j.applthermaleng.2011.07.033.

[40] N. Baydar and A. Ball, "A comparative study of acoustic and vibration signals in detection of gear failures using Wigner–Ville distribution," *Mech. Syst. Signal Proc.*, vol. 15, no. 6, pp. 1091–1107, 2001. DOI: 10.1006/mssp.2000.1338.

[41] K. Holmberg and A. Erdemir, "Influence of tribology on global energy consumption, costs and emissions," *Friction*, vol. 5, no. 3, pp. 263–284, 2017. DOI: 10.1007/s40544-017-0183-5.

[42] D. W. Sun, *Thermal Food Processing: New Technologies and Quality Issues*. Boca Raton, FL: CRC Press, 2005. DOI: 10.1201/9781420027372.

[43] A. K. Datta, "Porous media approaches to studying simultaneous heat and mass transfer in food processes. I: problem formulations," *J. Food Eng.*, vol. 80, no. 1, pp. 80–95, 2007. DOI: 10.1016/j.jfoodeng.2006.05.013.

[44] I. Pop and M. Sheremet, "Free convection in a square cavity filled with a Casson fluid under the effects of thermal radiation and viscous dissipation," *HFF*, vol. 27, no. 10, pp. 2318–2332, 2017. DOI: 10.1108/HFF-09-2016-0352.

[45] M. M. Ali, R. Akhter and M. A. Alim, "Performance of flow and heat transfer analysis of mixed convection in Casson fluid filled lid driven cavity including solid obstacle with magnetic impact," *SN Appl. Sci.*, vol. 3, no. 2, pp. 1–15, 2021. DOI: 10.1007/s42452-021-04243-x.

[46] S. Hussain, S. Shoeibi and T. Armaghani, "Impact of magnetic field and entropy generation of Casson fluid on double diffusive natural convection in staggered cavity," *Int. Commun. Heat Mass Transf.*, vol. 127, pp. 105520, 2021. DOI: 10.1016/j.icheatmasstransfer.2021.105520.